Ab initio simulations of tetrahedral amorphous carbon

N. A. Marks, D. R. McKenzie, and B. A. Pailthorpe
School of Physics, University of Sydney, Sydney, New South Wales 2006, Australia

M. Bernasconi and M. Parrinello
Max-Planck-Institut für Festkörperforschung, Stuttgart, D-70569, Germany
(Received 13 February 1996; revised manuscript received 21 May 1996)

Simulations are reported of a highly tetrahedral amorphous carbon network at a density of 2.9 g/cm^3 using Car-Parrinello first principles molecular dynamics. The network was generated by cooling a liquid carbon sample of 64 atoms to form an amorphous structure. The simulated structure is in good agreement with recent neutron diffraction data and contains 65% fourfold- and 35% threefold-coordinated carbon sites. Three- and four-membered rings are present in the structure and give the network an unusual topology. Evidence from neutron diffraction and organic chemistry is shown to support the existence of these ring structures, which resemble the carbon compounds cyclopropane and cyclobutane. Two additional networks were produced using different cooling rates. It was found that the number of fourfold sites decreased as the cooling time increased. This result has implications for the interpretation of experiments and models of how tetrahedral amorphous carbon is formed. [S0163-1829(96)03338-3]

I. INTRODUCTION

A number of amorphous forms of carbon are known to exist, including amorphous carbon,[1,2] glassy carbon,[3] and tetrahedral amorphous carbon.[4–6] With properties intermediate between diamond and graphite, tetrahedral amorphous carbon (*ta*-C) is extremely hard, has a density of approximately 3 g/cm^3, and is a weak *p*-type semiconductor. Potential applications for *ta*-C include wear-resistant coatings and thin-film semiconductor devices.

Unlike amorphous carbon (*a*-C), which consists almost entirely of threefold-coordinated (sp^2 bonded) atoms, *ta*-C contains a large fraction of fourfold-coordinated sites. Electron energy loss spectroscopy[7] has shown the fraction of fourfold-coordinated (sp^3-bonded) atoms is as high as 80–85%, with the remaining atoms being sp^2 hybridized. The combination of sp^2 and sp^3 sites means the structure of *ta*-C differs from the ''random tetrahedral networks'' formed by other group-IV materials such as amorphous silicon (*a*-Si) and amorphous germanium (*a*-Ge). In these materials all the atoms are tetrahedrally bonded (sp^3 hybridized), with threefold-coordinated sites representing dangling bonds.[8] The presence of sp^2 sites in *ta*-C distinguishes it from *a*-Si and *a*-Ge, and in this respect the structure of *ta*-C can be viewed as a random tetrahedral network with a contamination of sp^2 bonding. However, despite progress in establishing the basic structure of *ta*-C, a satisfactory structural model has yet to be found.

In a recent paper[9] we presented a short report of the first fully *ab initio* molecular dynamics (MD) calculation of a *ta*-C network in the scheme developed by Car and Parrinello.[10,11] The *ta*-C network, which was generated by cooling a liquid carbon sample, was found to contain a significant number of three- and four-membered rings. These small rings, which resemble the organic compounds cyclopropane (C_3H_6) and cyclobutane (C_4H_8), gave the network an unusual topology.

In this paper we perform further analysis of the *ta*-C structure, and present evidence from neutron diffraction and organic chemistry supporting the observation of the three- and four-membered rings. We also analyze the transition between the liquid and the amorphous solid and find that the sp^3 fraction is dependent on the rate at which the liquid is cooled. The observation that the sp^3 fraction decreases as the cooling time increases has important implications for interpretation of experiment.

A. Experimental background

A variety of techniques have been used to grow *ta*-C, including cathodic arc deposition,[12,13] ion-assisted deposition,[14,15] and mass-selected ion beam deposition.[16] Common to these approaches is the principle of energetic ion deposition, whereby a beam of energetic carbon ions is used to deposit a thin film of *ta*-C. It is well established that the ion energy strongly influences the properties of the films, and it has been shown that the sp^3 fraction is highest when the ion energy lies between 40 and 500 eV. A number of other film properties are dependent on the ion energy, including the resistivity, the density, and the compressive stress. This last property is particularly important as the compressive stress can be as high as 10 GPa, which is sufficient to cause delamination if the film thickness exceeds several hundred nm.

This link between the compressive stress, the sp^3 fraction, and the ion energy has been explored by several authors,[17–20] and a number of models have been proposed. Common to all models is the role played by the phenomenon known as a ''thermal spike.'' This term refers to the localized melting at the surface which occurs as a result of the impact of an energetic ion. The thermal spike is short lived as the energy rapidly diffuses away and the surface quickly cools to form a solid structure. It is this aspect of the deposition process which the liquid quench method used in this simulation seeks to emulate.

In the models of *ta*-C film growth, it is generally agreed that the thermal spike results in an annealing process which reduces the sp^3 fraction at high ion energies. However, the mechanism by which the thermal spike reduces the sp^3 fraction has not been established. In Sec. III G we present results showing that the *cooling rate* of the thermal spike is an important parameter which influences the sp^3 fraction. With this result we are able to explain why the sp^3 fraction progressively decreases when the ion energy is increased above several hundred eV.

B. Review of simulations

A number of attempts have been made to simulate the structure of *ta*-C using molecular dynamics. These have varied in accuracy and system size, and have used a variety of schemes, including the Tersoff potential,[21] the tight-binding approximation,[22,23] and local orbital *ab initio* methods.[24] The fully *ab initio* Car-Parrinello technique used in this work has not been previously applied to *ta*-C.

The least accurate of the techniques listed above is the empirical Tersoff potential[21] which is parametrized to fit the elastic constants of graphite and diamond. Despite its inherent limitations, Kaukonen and Nieminen[25] had some success modeling the deposition of carbon films using this potential. In agreement with experiment, they found that the films were most diamondlike when the ion energy was in the range 40–70 eV. However, their maximum sp^3 fraction was 44%, considerably lower than the experimentally observed value.

Kelires[26] also used the Tersoff potential in conjunction with a Monte Carlo annealing algorithm to generate amorphous carbon (*a*-C) structures at a range of densities. With increasing density, the sp^3 fraction rose from 10% up to a maximum of 90%. Kelires also calculated an atomic level stress and found that in the *ta*-C structure the sp^3 atoms were predominantly compressively stressed, while the sp^2 atoms were mainly under a tensile stress.

More transferable than the Tersoff potential, the tight-binding model has been used by Wang and Ho[22] in simulations of *a*-C. They generated a range of structures with densities from 2.2 up to 3.4 g/cm^3, and with increasing density they too observed an increase in the sp^3 fraction. However, the structure generated at a density of 3 g/cm^3 did not compare well with experiment, containing just 33% sp^3 sites and even a small number (2.3%) of *sp*-bonded atoms. A higher sp^3 fraction was obtained by quenching the liquid at the higher density of 4.4 g/cm^3, and later rescaling the network to 3.4 g/cm^3. After an annealing cycle the structure contained 89% fourfold sites and 11% threefold sites. An increase in the quenching rate of the liquid (from 5×10^{14} K/ps to 10^{15} K/ps) did not affect the sp^3 fraction of a structure generated at a density of 3.35 g/cm^3.

Frauenheim *et al.*[23] performed simulations with a nonorthogonal tight-binding scheme. A number of carbon networks were generated, and as the density was changed from 2 to 3.5 g/cm^3 the sp^3 fraction increased from 9% to 88%. The π-π^* gap was approximately 3 eV for structures at a density of 3.0 and 3.3 g/cm^3, while the gap in a 3.52 g/cm^3 structure was over 5 eV. Weak bonds between threefold sites separated by a distance greater than 1.8 Å were also found to saturate defect states in the 3.0 g/cm^3 structure. The density of defect states at the Fermi level is therefore minimal for the 3.0 g/cm^3 structure which appears to be particularly stable, having the lowest energy among the samples simulated.

The most sophisticated technique used prior to this work is the local orbital *ab initio* method proposed by Sankey and Niklewski.[27] Containing no empirical terms, the scheme uses pseudopotentials within density functional theory. However, the calculation is not self-consistent, and the minimal basis set of atomic orbitals is used. When Drabold *et al.*[24] applied the local orbital *ab initio* method to *ta*-C they generated a 3 g/cm^3 structure with an sp^3 fraction of 85%. They observed that the sp^2 atoms paired up and reported a defect-free band gap of 2 eV, in agreement with experiment.

While the techniques discussed above have had varying degrees of success, each method contains approximations designed to increase the computational efficiency. These approximations are usually justified by demonstrating that the scheme reproduces known properties of several crystalline or molecular structures. However, this ability is no guarantee that the model will be sufficiently flexible to reproduce the wide variety of bonding environments present in an amorphous material such as *ta*-C. For example, Wang and Ho have stated[28] that the tight-binding approximation does not predict the correct cohesive energy for simple cubic structures. This means that networks containing bond angles less than 90° will not be well described by their tight-binding method.

The *ab initio* technique used in this work represents an advance over these previous simulations as the Car-Parrinello formalism is essentially exact within density functional theory in the local density approximation (LDA). The scheme is self-consistent and uses an unbiased basis set. On these grounds we believe the fully *ab initio* Car-Parrinello technique to be the most suitable computational technique for investigating *ta*-C.

II. COMPUTATIONAL DETAILS

The simulation system contained 64 atoms at a density of 2.9 g/cm^3 (Ref. 29) in a simple cubic supercell whose volume remained constant throughout the simulation. Recent electron spin resonance (ESR) measurements[30] of *ta*-C have shown that the density of unpaired spins is less than 1 unpaired spin for every 50 sp^2 atoms. Therefore no unpaired spins are expected in the sample and the use of the local density approximation[31] (LDA) instead of the local spin density (LSD) approximation is justified. A Car–von Barth norm-conserving pseudopotential in the Kleinman-Bylander form was used.[32] The electronic wave functions were expanded in plane waves up to a kinetic energy cutoff of 35 Ry and an integration time step Δt of 3 a.u. (0.072 fs) was used.

During the equilibration of the liquid and solid structures a Nosé thermostat[33] was used to control the ion temperature. The characteristic frequency for the thermostat was 1250 cm^{-1}, which lies close to the peak at 37 THz in the diamond phonon density of states.[34] The Nosé thermostat was not used during the cooling of the liquid. The cooling of the liquid was controlled by a velocity rescaling algorithm acting in discrete steps, reducing the temperature from 5000 to 300 K in 14 stages. At each stage a target temperature T_0 was

defined, and if the temperature differed from T_0 by more than the fluctuations expected for the microcanonical ensemble of our system, the ion velocities were rescaled to bring the temperature back to T_0.

A second Nosé thermostat[35] was used to control the fictitious electronic kinetic energy. This thermostat prevented the electronic wave functions from drifting away from the instantaneous ground state (the Born-Oppenheimer surface), by removing excess fictitious kinetic energy. This drift is particularly severe for metals.[36] In our simulation the liquid carbon sample possesses no band gap and hence the energy transfer rate is high. The characteristic frequency for the thermostat was 45 000 cm^{-1} and the target kinetic energy $E_{kin,0}$ was chosen according to the prescription in Ref. 35. The Nosé thermostat on the electrons was used throughout the simulation and proved to be an effective way of keeping the electrons on the Born-Oppenheimer surface. During the equilibration of the liquid, the cooling of the liquid, and the temporal averaging of the solid, the deviation from the Born-Oppenheimer surface was never more than 0.01 eV/ion, and was often much less.

The initial configuration of the atoms was a simple cubic lattice with random displacements up to 0.2 Å in amplitude. This structure is highly unstable for carbon and melted spontaneously without the addition of any kinetic energy. Within 0.02 ps the simple cubic lattice was destroyed, the temperature had risen to 6000 K, and the liquid began to diffuse. At this point a quench to the Born-Oppenheimer surface was performed and the Nosé thermostats on both the ions and the electrons were activated. Now molten, the liquid was equilibrated at 5000 K for 0.36 ps where it was highly diffusive, the diffusion coefficient being 7.1×10^{-5} cm^2/s.

The liquid sample was then cooled to 300 K over 0.5 ps, corresponding to a cooling rate of 10^{16} K/s. Following this the system was equilibrated for a further 0.5 ps to gain temporal averages. Two further simulations were performed to study the effect of varying the cooling rate. One simulation used a slower cooling rate while in the other the liquid was cooled instantly to 300 K.

III. RESULTS

A. General properties of the *ta*-C structure

The final annealed structure contains 22 threefold-coordinated atoms, which we shall refer to as sp^2 hybridized, and 42 fourfold-coordinated atoms, which we refer to as sp^3 hybridized. The coordination was determined by counting the number of atoms lying within 1.85 Å of an atomic site, a definition which is used for the remainder of this paper. A significant feature of the structure is the frequent occurrence of three- and four-membered rings which give the network an unusual topology. Through the presence of these structures even the tetrahedrally bonded part of the network differs substantially from the silicon tetrahedral network inferred from experimental data[8] as well as from *ab initio* simulations.[37]

Some of the basic structural parameters of the network are shown in Table I. For comparison, experimental results for *ta*-C prepared by cathodic arc deposition[38] are included in the table. The simulated structure is in good agreement with experiment at this density, particularly with regard to the nearest-neighbor distances r_1 and r_2. The sp^3 fraction is also in satisfactory agreement with experiment as the experimental uncertainty is of the order of 10%. The present structure has the highest sp^3 content of any carbon network simulated with the Car-Parrinello technique. Previous work,[39] using a density of 2 g/cm^3, produced a pure carbon network with a sp^3 fraction of 15%, and more recently a hydrogenated carbon network[40] at a density of 2.6 g/cm^3 was found to have an sp^3 fraction of 56%. Our results at a density of 2.9 g/cm^3 confirm that *ab initio* simulations reproduce the experimentally known increase in sp^3 fraction with density.

TABLE I. Comparison between structural parameters of simulated *ta*-C (this work), and experimentally prepared *ta*-C.

Quantity	Simulated network	Experiment	Ref.
First-nearest-neighbor distance r_1(Å)	1.52	1.52 1.53	38 5
Second-nearest-neighbor distance r_2(Å)	2.50	2.50	5
First coordination number N_1	3.65	3.93	5
Second coordination number N_2	9.65	8.9–10.0	5,6
sp^3 fraction	0.65	0.80	4

The internal stress of the structure was calculated using the technique of Bernasconi *et al.*[41] which corrects for the so-called Pulay stress.[42] The stress was compressive and measured approximately 5 GPa in magnitude, a value which compares well with experiment. In addition, the stress was highly anisotropic, with the diagonal components of the stress tensor equaling $(-6,6,15)$ GPa. To confirm the stability of the structure, the network was relaxed at a constant pressure of 5 GPa using the technique of Ref. 41. The relaxed structure was then compared with the constant volume network using the pair distribution function $g(r)$, which is discussed in a later section. It was found that the $g(r)$ of the two structures were indistinguishable, demonstrating that the *ta*-C network represents a stable structure.

B. Ring structures

Figure 1 shows just the three- and four-membered rings present in the *ta*-C structure. Although the presence of such small rings seems at first surprising, the hydrogenated analogues of these rings, known as cycloalkanes, are well described and stable. As shown in Fig. 1, cyclopropane (C_3H_6) contains a ring of three sp^3-bonded carbon atoms, and cyclobutane (C_4H_8) contains a ring of four. The departure of the bond angle from the ideal sp^3 value of 109.47° produces considerable strain in both structures. An estimate of this strain energy is given in Table II which compares some common cycloalkanes to cyclohexane, which is essentially strain free. The energies were calculated using the heat of formation per CH_2 group,[43] and are quoted relative to cyclohexane where the carbon bond angle is 109.47°. We note that these strain energies include a small interaction between hydrogen atoms, and hence the strain energy asso-

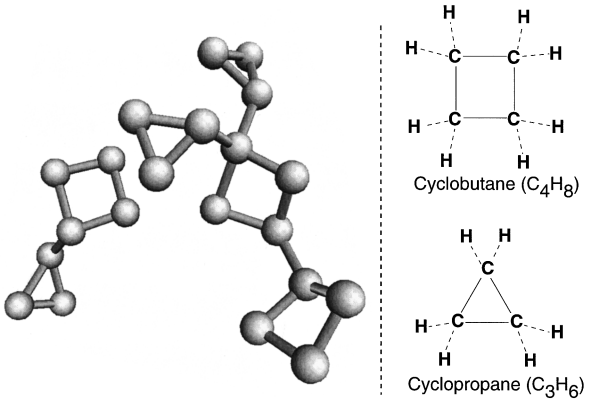

FIG. 1. Left: view showing only the three- and four-membered rings present in the *ta*-C structure. All the atoms are sp^3 hybridized. Right: the organic elements cyclopropane and cyclobutane.

ciated with the bending of the carbon-carbon bonds is slightly lower than the values quoted in Table II.

It is evident that the five- and seven-membered rings are significantly less strained than the three- and four-membered rings. While the strain energies of cyclopropane and cyclobutane are reasonably high, experiments show that *ta*-C is formed only in the presence of a compressive stress, which would both promote and stabilize such strained structures. In addition, the increased density of the three- and four-membered rings would compensate for the strain energy cost by allowing the surrounding atoms to form lower density, and less-stressed, structures. In contrast to the highly stressed *ta*-C, amorphous carbon films are less dense and have a much lower stress, and both experiments[44] and *ab initio* simulations[39] have shown it to consist primarily of five-, six-, and seven-membered rings, which incur a low strain energy cost.

The distribution of ring sizes provides a useful means of comparing networks, and Table III shows the ring statistics for this work and the simulations of Wang and Ho[22] and Frauenheim *et al.*[23] It is evident that the structure presented in this work differs considerably from previous simulations of *ta*-C, particularly with regard to the number of three- and seven-membered rings. In the simulations of Wang and Ho, no three- and four-membered rings are present in any of the structures, and the sp^3 fraction at 3 g/cm^3 is too low. It is interesting that even though the 3.3 g/cm^3 network has an sp^3 fraction similar to this simulation, the topology is completely different. In the simulations of Frauenheim *et al.*, the

TABLE II. Strain energies (Ref. 43) for some common cycloalkanes $(CH_2)_n$. The strains are calculated using the heat of formation and are measured relative to cyclohexane which is essentially strain free.

n	Cycloalkane $(CH_2)_n$	Strain energy of molecule (eV)	Strain energy per C atom (eV)
3	cyclopropane	1.17	0.39
4	cyclobutane	1.13	0.28
5	cyclopentane	0.26	0.05
6	cyclohexane	0	0
7	cycloheptane	0.26	0.03

TABLE III. Ring statistics for this work and other simulations of *ta*-C. The ring statistics for the 128- and 216-atom structures have been normalized to 64 atoms for the purposes of comparison. The three highest-density networks generated by Wang and Ho were quenched at higher densities and subsequently rescaled to the densities shown.

	Number of atoms	Density (g/cm^3)	sp^3 (%)	Number of rings 3	4	5	6	7
This work	64	2.9	65	3	3	21	19	9
Frauenheim *et al.*[a]	64	3.0	53	0	0	20	21	20
	64	3.3	83	0	1	28	33	39
	128	3.0	64	0	3	18	27	16
	128	3.3	75	0	3	20	30	27
	128	3.52	88	0	3	21	40	34
Wang and Ho [b]	216	3.0	33	0	0	10	17	10
	216	3.3	59	0	0	17	27	17
	216	3.35	74	0	0	16	41	29
	216	3.4	89	0	0	21	45	38

[a]Reference 23.
[b]Reference 22.

sp^3 fraction at 3 g/cm^3 is similar to this work. However, no three-membered rings are present and the number of seven-membered rings is significantly greater. We also note that while the 128-atom structures contain four-membered rings as observed in this simulation, the 64-atom networks do not follow the same trend.

C. Structural analysis

The radial distribution function $G(r)$ provides a useful means of comparison of the simulated structure with experiment. $G(r)$ is defined by

$$G(r)=4\pi r[\rho(r)-\rho_0], \tag{1}$$

where $\rho(r)$ is the density of atom centers at a distance r from an atom, averaged over the network, and ρ_0 is the average density. We show in Fig. 2 the $G(r)$ calculated from the simulation and a recent neutron diffraction result.[6] The

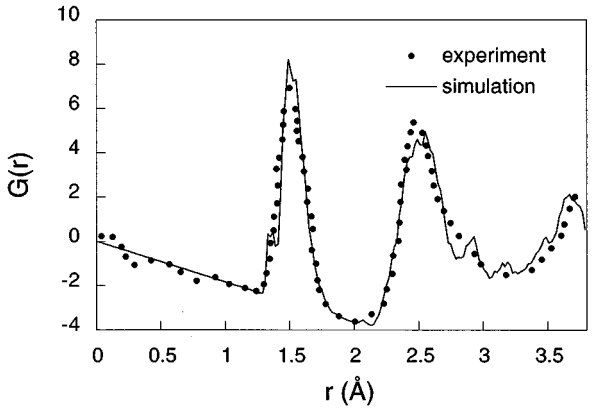

FIG. 2. The radial distribution function $G(r)$ calculated for the simulated *ta*-C structure shown as a solid curve, compared with neutron diffraction results (Ref. 6) (dotted curve). The simulated $G(r)$ is a temporal average over 0.5 ps at 300 K.

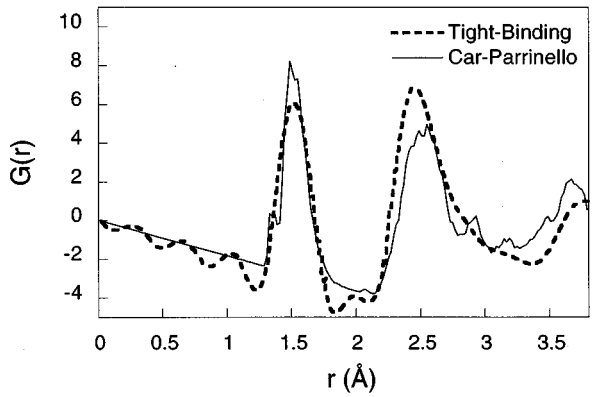

FIG. 3. Comparison between ta-C structures simulated using the Car-Parrinello technique (this work) and the tight-binding approximation (Ref. 22).

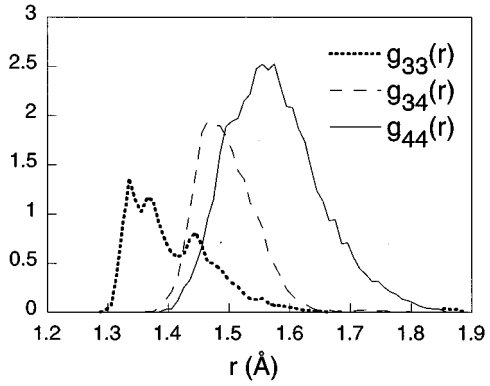

FIG. 4. The partial distribution functions $g_{ij}(r)$ for the first peak of the simulated structure. The subscripts i and j denote the coordination of the atoms.

agreement is good in both the position and shape of the first two coordination peaks. The third principal peak (near 3.7 Å) shows some discrepancies which are probably due to the finite size of the simulation cell. The strong asymmetry observed experimentally for the second peak agrees well with the presence of subsidiary features in the $G(r)$ for the simulated network at large r. When subject to experimental broadening these features should give rise to the observed asymmetry.

The agreement between experiment and our simulated structure seen in Fig. 2 is currently the best in the literature. Other simulations fail to reproduce experimentally observed features such as the relative heights of the first two peaks in $G(r)$. An example of this is seen in Fig. 3 which compares this work with a ta-C structure generated by Wang and Ho[22] using the tight-binding approximation. In the tight-binding simulation, the second peak of $G(r)$ is higher than the first peak, in contrast to both experiment and the Car-Parrinello simulations in this work, where the converse is the case. This difference indicates that the tight-binding method does not provide a complete description of the unusual topology present in ta-C. In the tight-binding simulations performed by Frauenheim *et al.*,[23] the situation is similar, with the second peak in $G(r)$ being higher than the first.

The pair distribution function $g(r)$ is another useful tool for structural analysis, and is defined by

$$g(r)=\frac{\rho(r)}{\rho_0}. \tag{2}$$

Figure 4 shows the three partial distribution functions comprising the first peak in $g(r)$ of the simulated ta-C structure. The quantities $g_{33}(r)$, $g_{34}(r)$, and $g_{44}(r)$ correspond to pure sp^2, hybrid sp^2/sp^3, and pure sp^3 distances, respectively. All three distributions are considerably broad and contribute to the substantial width of the first peak. The width of the individual distributions is due to a number of factors including strain in the structure, different topologies, variations in bond order, and thermal broadening. We note that the g_{33} distribution does not have the symmetry present in g_{34} and g_{44}. This asymmetry is a consequence of variations in the bond order and the reasons for this are discussed later in this section. Another feature of Fig. 4 is the increase in the bond length with coordination number, with the average bond lengths for the three distributions being 1.413, 1.500, and 1.584 Å, respectively.

D. Second-neighbor coordination

It is of interest to examine the number of second nearest neighbors, defined as atoms not bonded to each other but bonded to a common third atom. In particular it is possible to resolve an experimental discrepancy raised by Gilkes *et al.*[6] concerning the second coordination number of ta-C. They reported that the number of second nearest neighbors, N_2, was too small relative to the first coordination number N_1 by approximately 30%. This deficiency was based on the relation

$$N_2=N_1(N_1-1), \tag{3}$$

which is described in the literature as being appropriate for a fully bonded network with a minimum ring size of 5. However, as demonstrated in the Appendix, the correct expression for such a network is instead

$$N_2=6(N_1-2), \tag{4}$$

but applying this corrected formula does not remove the discrepancy.

In the analysis of Gilkes *et al.* the coordination numbers were calculated by fitting Gaussians to the experimental $G(r)$ and integrating over r. Table IV shows the distances, standard deviations, and coordination numbers for the first few peaks. The discrepancy they report is between $N_1=3.90$ (from the peak at 1.52 Å) and $N_2=7.66$ (from the peak at 2.48 Å). Using the correct relationship [Eq. (4)], the expected value of N_2 would be 11.40, somewhat larger than 7.66. To resolve this difference Gilkes *et al.* proposed that most of the atoms in the peak at 2.75 Å are actually second nearest neighbors, implying an asymmetric second-neighbor distribution. However, our analysis shows that the second-neighbor distribution is in fact symmetric and that the N_2 discrepancy is attributable to two other factors.

The first factor is that the second-neighbor distribution is broader than the 0.13 Å reported by Gilkes (see Table IV). In Fig. 5 we show the pair distribution functions $g(r)$ and

TABLE IV. Average atomic distances r, standard deviations σ, and coordination numbers N for experimentally prepared ta-C. The values were obtained by fitting a superposition of Gaussians to the experimental $G(r)$. The data shown in this table is taken from Table I of Gilkes *et al.* (Ref. 6).

r (Å)	σ (Å)	N
1.52	0.11	3.90
2.15	0.11	0.24
2.48	0.13	7.66
2.75	0.14	4.37
3.00	0.13	3.06

$g_2(r)$, where $g(r)$ is defined as in Eq. (2), and $g_2(r)$ is defined in a similar way but counts only distances between second nearest neighbors. This definition of $g_2(r)$ includes only those distances between atoms which are not bonded to each other, but are bonded to a common third atom. It is clear from Fig. 5 that the second neighbors have an extremely broad distribution, extending from 2 Å up to 3.2 Å, and have a significant overlap with third nearest neighbors. This large width in $g_2(r)$ means it is difficult to extract the second-neighbor distribution from the experimental $G(r)$.

In Fig. 6 the second-neighbor distribution (solid circles) is shown to be well fitted by a Gaussian (thin line). This demonstrates that the second-neighbor distribution is in fact symmetric and implies that the asymmetry in the second peak of the experimental $G(r)$ is due to the third nearest neighbors. It is also evident that the standard deviation σ reported in Table IV is lower than the 0.16 Å seen in Fig. 6. This lower value of σ is responsible for much of the N_2 discrepancy and illustrates the difficulty of deconvoluting the second coordination peak from experimental data.

The second reason for the N_2 discrepancy is that the three- and four-membered rings in the network reduce the number of second neighbors relative to N_1. In the case of our structure (where $N_1=3.65$), the value of N_2 predicted by Eq. (4) is 9.90 compared to the actual value of 9.65. This difference is due entirely to the presence of three- and four-membered rings.

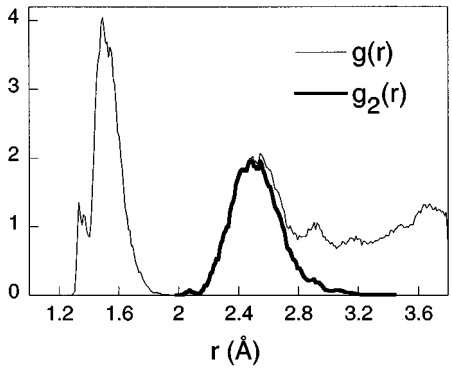

FIG. 5. Comparison between the pair distribution functions $g(r)$ and $g_2(r)$ of the simulated ta-C structure. $g(r)$ (thin line) shows the distribution of all distances in the structure, whereas $g_2(r)$ (solid line) shows the distribution of just the second nearest neighbors.

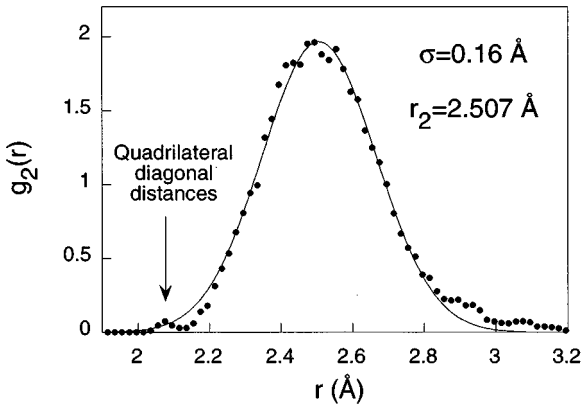

FIG. 6. The second-neighbor distribution function $g_2(r)$ (solid circles) fitted with a Gaussian curve (thin line). r_2 and σ are the average bond length and standard deviation of the curve fit, respectively. The peak indicated by the arrow is due to diagonal distances across cyclobutanelike quadrilaterals.

The data in Table IV provide direct confirmation that the cyclobutanelike quadrilaterals are present in experimentally prepared ta-C. The table reports a peak in the experimental $G(r)$ at 2.15 Å, a distance which corresponds to the diagonal distance across a quadrilateral. This length can be identified as due to quadrilaterals alone as such a short second-neighbor distance cannot be generated by any other structure. Figure 6 shows that the simulated structure has a similar peak at 2.10 Å, and analysis of the structure shows that all the distances contributing to this peak are diagonal distances across quadrilaterals. The coordination number N provides further support for this interpretation. Calculation of the simulation coordination number yields a value of 0.19 which compares very favorably with the experimental value of 0.24 in Table IV.

E. Electronic properties

The computed electronic density of states (DOS) of the simulated structure was calculated and is shown as Fig. 4 of Ref. 9. As would be expected, the π and π^* peaks, which reflect the amount of sp^2 bonding, are not as pronounced as in the amorphous carbon sample of Galli *et al.*[39] and this has the effect of widening the band gap. As is typical for amorphous materials, it is difficult to measure the band gap from the DOS due to the presence of states near the Fermi energy (0 eV). A useful measure of the gap can be obtained by calculating the ''Tauc band gap''[45] using the imaginary part of the dielectric permittivity, $\epsilon_2(\omega)$. The process of calculating $\epsilon_2(\omega)$ for the simulated structure is a straightforward one[46] involving a convolution of the occupied and unoccupied densities of states, provided one makes the assumption that the matrix elements for dipole transitions are independent of energy. The calculation yielded a Tauc band gap of 0.5 eV, which is an underestimate due to the use of the local density approximation. Comparison with experiment is not straightforward, as the commonly accepted experimental value[47] of 2.5 eV is somewhat uncertain because the experimental Tauc plot for ta-C shows deviations from the linear

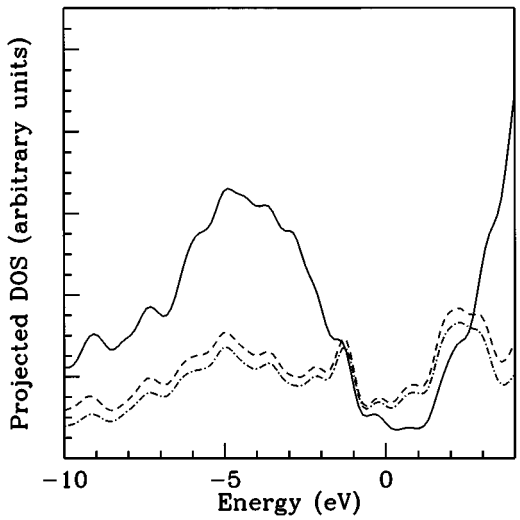

FIG. 7. Electronic density of states projected on the minimal basis set of atomic orbitals. The solid and dashed lines correspond to projections on the atomic orbitals of the sp^3 and sp^2 atoms, respectively. The dash-dotted line is the DOS projected on the p orbitals only of the sp^2 atoms. In the π-π^* gap region (see Fig. 4 of Ref. 9.) The states are mainly p-like localized in the sp^2 region. Due to nonorthogonality of the basis set, the sum of the DOS's projected on sp^2 and sp^3 sites does not equal the total DOS's in Fig. 4 of Ref. 9. A Gaussian with a standard deviation of 0.3 eV has been used to smooth the data.

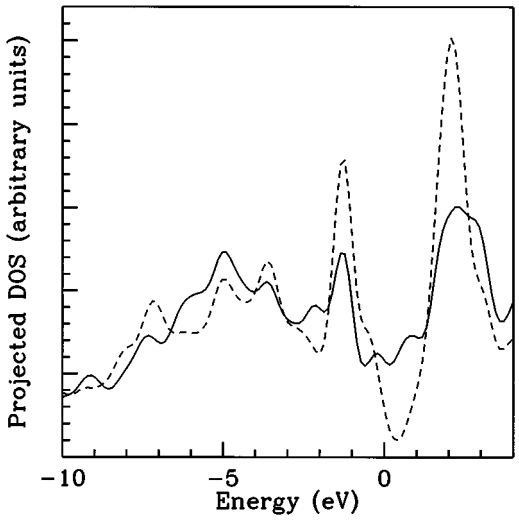

FIG. 8. Electronic density of states projected on the atomic p orbitals of the sp^2 atoms. Solid line: projection on all the sp^2 atoms, normalized to the number of atoms (22). Dashed line: projection on the isolated sp^2 dimers in Fig. 9, normalized to the number of atoms (4). The two sharp peaks below and above the Fermi level in the DOS projected on the dimers are bonding and antibonding ethylenic states.

behavior typical of amorphous semiconductors. In addition, recent experiments by Schwan *et al.*[48] measured a Tauc gap in ta-C of less than 1 eV.

In order to obtain some qualitative information on the nature of the states in the gap we projected the Kohn-Sham orbitals on the minimal basis set of atomic orbitals. In Fig. 7 the DOS's projected on the atomic orbitals of the sp^2 and sp^3 atoms are compared. The states which contribute to the DOS in the π-π^* gap are mainly localized in the sp^2 region and are predominantly π-like. It is also interesting to consider the electronic properties of particular sp^2-bonded atoms. In the ta-C structure the sp^2 atoms form small clusters of various sizes. In two instances, ''isolated'' sp^2 dimers are present, and these produce distinct bonding and antibonding ethylenic states. These are visible as sharp peaks below and above the Fermi level in Fig. 8, where the DOS's projected on the p orbitals of the sp^2 atoms and of the sp^2 dimers only are compared. Further evidence for the ethylenic nature of these sp^2 atoms is presented below. Note that the projected DOS's in Fig. 8 are normalized to the number of atoms used in the projection.

F. Properties related to sp^2 atoms

Figure 9 shows only the sp^2 atoms in the structure and demonstrates there is a strong tendency for the sp^2 atoms to cluster. The two sets of sp^2 dimers discussed above are also evident. A measure of the clustering was obtained by calculating the ratio n_{33}/n_{34}, where n_{33} is the number of sp^2-sp^2 bonds and n_{34} is the number of sp^2-sp^3 bonds. A ratio of 0.60 was calculated for the ta-C structure, considerably larger than the value of 0.25, indicative of a homogeneous distribution of sp^2 sites.

It is interesting that no isolated threefold atoms are present in Fig. 9, as an isolated threefold atom in an sp^3 network could induce the formation of a dangling bond sp^3-like or sp^2-like (p_z-like). In the LDA only doubly occupied or empty dangling bonds are possible, and the LDA would therefore reproduce the effective negative Hubbard-U model of dangling bonds proposed for a-Si and a-Ge.[8] While the LSD approximation would allow singly occupied dangling bonds at the Fermi level, ESR measurements[30] show that most of the spins in ta-C are paired.[49] Our results therefore confirm that the threefold-coordinated atoms do not act as effective negative Hubbard-U centers, but are instead mainly sp^2-like. They cluster in order to produce ethylenic or conjugated bonding states from the p_z ''dangling bonds.'' This clustering effect has been pointed out also in Refs. 23 and 24.

The tendency of the sp^2 sites to cluster has consequences for the electrical conductivity of ta-C. When the sp^2 chains

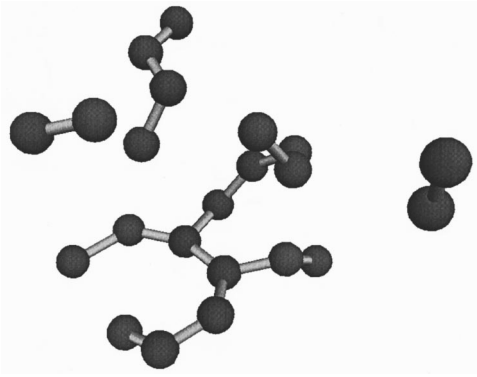

FIG. 9. The ta-C network showing just the 22 sp^2 hybridized atoms. The structure contains four unlinked chains of sp^2 atoms containing 2, 2, 4, and 14 atoms.

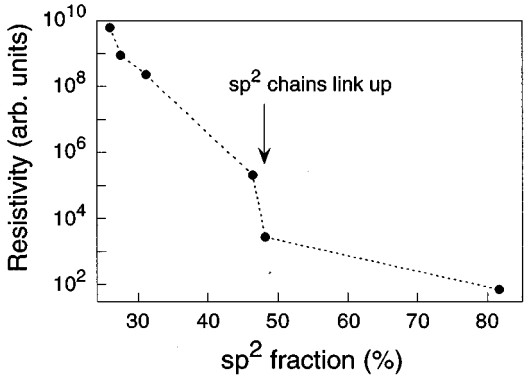

FIG. 10. Resistivity in Xe-implanted *ta*-C as a function of sp^2 fraction. Data taken from Ref. 50.

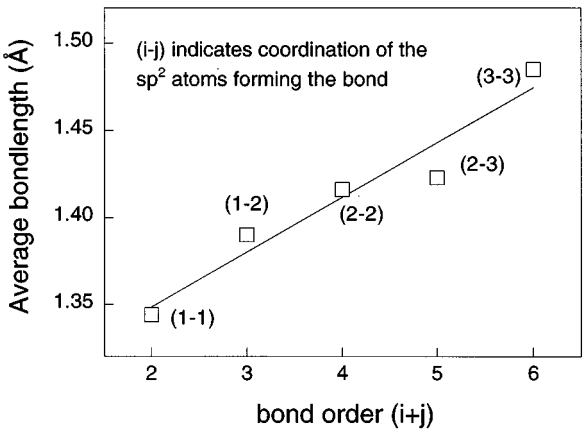

FIG. 11. Average distances between sp^2 atoms as a function of the bond order defined in the text. The bracketed numbers $(i\text{-}j)$ indicate the sp^2 coordination of the five distance categories.

are isolated (as they are in Fig. 9), only hopping conduction can occur. However, should the chains link up, extended state conduction along the sp^2 chains would dramatically increase the electrical conductivity. This effect has been observed in ion implantation studies[50] where 10 keV Xe ions were used to progressively damage *ta*-C. With increasing dose the sp^2 fraction increased from 26% to 82%, producing an eight orders of magnitude decrease in the resistivity. Figure 10 shows the dependence of the resistivity on the sp^2 fraction and demonstrates that between 22% and 46% sp^2 fraction the resistivity decreased relatively slowly. However, when the sp^2 fraction increased from 46% to 48%, the resistivity dropped two orders of magnitude. This sudden drop can be identified as the point at which the sp^2 chains link up and form a connected network.

With an sp^2 fraction of 35%, the simulated *ta*-C structure lies below the critical sp^2 concentration. However, the addition of a small number of sp^2 atoms would enable the chains to link up. An additional eight sp^2 atoms, for example, would increase the sp^2 fraction to 47% and could well result in the linking of the sp^2 chains. This would produce the sudden drop in the resistivity observed experimentally. While this argument is qualitative, it demonstrates that the simulated structure is consistent with experimental data and provides a visual picture of experiment.

The sp^2 atoms also occur in a variety of bonding environments ranging from pairs of sp^2 atoms with ethylenelike double bonds, to extended structures containing some graphitelike sp^2 atoms. Analysis of the sp^2 network reveals that with increasing graphitelike character the distance between sp^2 atoms increases. This effect is a consequence of the decreased strength of the π bonding due to their delocalization in conjugated bonds. This effect is commonly described using the concept of bond order, which measures the strength of a bond.

To measure this dependence we use an empirical bond order parameter based on the number of other sp^2 sites each sp^2 atom is bonded to. We call this number the sp^2 coordination and define the bond order as the sum of the sp^2 coordinations of the two atoms forming the bond. Figure 11 shows the variation in the average sp^2-sp^2 distance with the bond order, and demonstrates the trend to increasing bond length with increasing bond order. This variation in the bond length with bond order is consistent with observed behavior in a variety of carbon compounds and explains the broad distribution of $g_{33}(r)$ seen in Fig. 4. We note that the (1-1) category, which describes isolated sp^2 dimers, has essentially the same bond length as ethylene where the carbon-carbon distance is 1.33 Å. The confirms the observation presented earlier that pairs of sp^2 atoms exhibit ethylenic-type bonding.

G. Varying the cooling rate

An important parameter identified in this work is the rate at which the liquid cools to the amorphous solid. To evaluate the effect of this parameter two further *ta*-C structures were produced by cooling the liquid to 300 K at different rates. Figure 12 shows the two additional cooling protocols, denoted ''instant'' and ''slow,'' as well as the ''fast'' cooling protocol which was used to produce the *ta*-C structure presented in Sec. III.

The three cooling profiles provided a range of conditions for the liquid-amorphous transition. Under the instant cooling profile the liquid was quenched instantaneously to 300 K and constrained to have a temperature in the range 300 ± 100 K. The structure produced was the least relaxed of

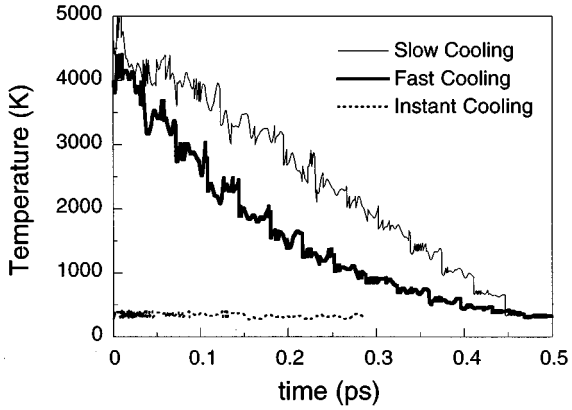

FIG. 12. The three temperature protocols used to cool the liquid. The *ta*-C structure presented in Sec. III was produced using the ''fast'' cooling protocol.

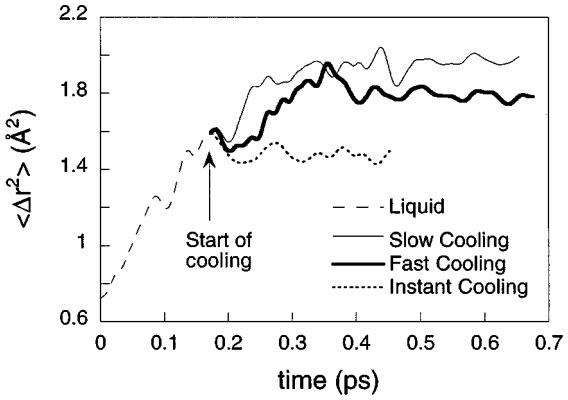

FIG. 13. The mean-square displacement $\langle \Delta r^2 \rangle$ as a function of time in the liquid and during the three cooling protocols. The amount of diffusion during the cooling process was greatest under the slow protocol, and least with the instant protocol.

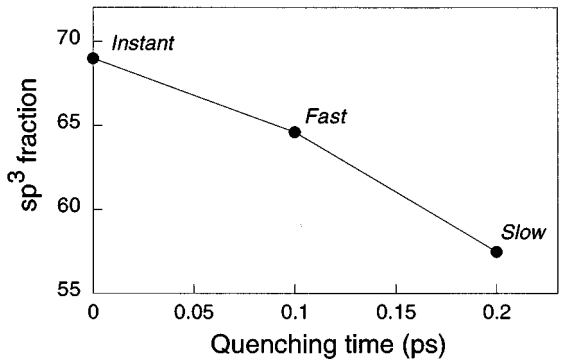

FIG. 14. The sp^3 fraction of the structures simulated using the three cooling protocols as a function of the quenching time. The quenching time is defined as the length of time the sample temperature is between 5000 and 3000 K. In the case of the instant cooling profile this time is zero.

the three, as the network was forced to conform to the disordered topology of the liquid. The other two cooling rates are more physically realistic and allowed the liquid time to seek a lower-energy minimum. Under the fast cooling profile the temperature fell exponentially from 5000 K to 300 K over 0.5 ps, whereas the decrease was linear for the slow profile.

The quantity most affected by the cooling rate was the fraction of sp^3 sites in the three samples. The liquid itself contained 60% sp^2 atoms, 31% sp^3 atoms, and 8% sp atoms. The structure produced using the instant cooling profile had the highest sp^3 fraction, with 69% of the atoms fourfold coordinated. This was followed by the fast structure examined in Sec. III which contained 65% sp^3 sites, while the slow cooling profile produced a structure containing just 57% sp^3 atoms.

This variation in sp^3 fraction can be related to the amount of diffusion taking place during the cooling process. To quantify the diffusion process we use the mean-square displacement (MSD), which is defined by

$$\mathrm{MSD}(t) = \langle [\mathbf{r}(t) - \mathbf{r}(0)]^2 \rangle, \tag{5}$$

where the average is taken over all 64 atoms. In a liquid the MSD increases linearly with time, indicative of diffusion taking place, whereas in a solid the MSD is constant over time as the average position of the atoms is fixed. Figure 13 shows the MSD for the three cooling protocols and the latter part of the liquid equilibration. While the liquid is molten the MSD shows the expected linear increase with time, but as the system is cooled the diffusion rate decreases and the MSD reaches a constant average value. The magnitude of this final value reflects the amount of diffusion after the cooling process began. It is evident that the greatest amount of diffusion occurred under the slow profile, followed by the fast profile, while under the instant protocol no diffusion occurred at all. This demonstrates that the length of time the system is diffusive determines the final structure.

A comparison of Figs. 12 and 13 reveals that the MSD attains its final average value after the sample has cooled to approximately 3000 K. In the case of the instant, fast, and slow protocols, the time taken to reach this temperature is 0, 0.1, and 0.2 ps, respectively. Based on this observation, we define a ''quenching time,'' an empirical quantity equal to the length of time the sample temperature is between 5000 and 3000 K. In Fig. 14 the sp^3 fraction of the three structures is shown as a function of this quenching time. This plot demonstrates the relationship between the sp^3 fraction and the amount of diffusion taking place during the solidification process. In the case of the instant profile, the atoms are unable to exchange positions due to their lack of kinetic energy. However, in the case of the fast and slow protocols, the diffusion which takes place during the cooling process allows the structure to achieve a lower-energy structure and a smaller sp^3 fraction.

The structural changes occurring during the cooling process are summarized in Fig. 15 which shows the fraction of sp, sp^2, and sp^3 sites as a function of time for the three cooling protocols. Common to all three graphs is a decrease in the number of sp^2 sites, an increase in sp^3 sites, and the disappearance of sp-bonded atoms.

It is interesting that the greatest change in coordination occurs under the instant profile, where the quenching time is the shortest and the least amount of diffusion occurs. This slightly paradoxical result can be understood considering the space-filling properties of the system. In the liquid state the atoms are distributed reasonably evenly throughout the simulation cell due to the high atom mobility. At the instant the liquid is cooled, this instantaneous structure favors sp^3-bonded atoms as they fill space more efficiently than sp^2 atoms. However, when the cooling time increases, and the amount of diffusion increases, a configuration energetically more acceptable to sp^2 atoms is generated. Note that the sp^2 network in the liquid, being favored by entropy, is different from the sp^2 network in the ta-C samples.

Despite having higher total energies, the samples with a higher sp^3 fraction were found to have lower compressive stresses. This slightly unexpected behavior is a consequence of the fixed size of the simulation cell. For example, if the sample pressure were fixed instead of the cell volume, the equilibrium density of the instant structure would be higher than the slow and fast structures, as a higher sp^3 fraction implies a higher density at constant pressure. However, in experimentally prepared ta-C the pressure and density vary

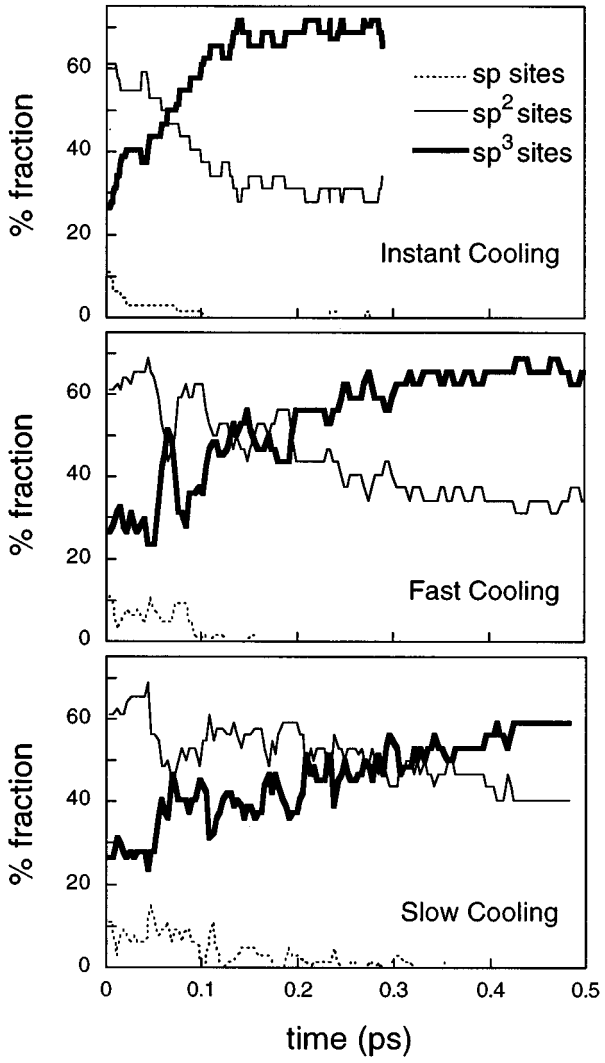

FIG. 15. Fraction of sp (dotted line), sp^2 (thin line), and sp^3 (thick line) sites as a function of time for the three cooling protocols.

simultaneously, and hence the dependence of the stress on the sp^3 fraction cannot be compared directly with the experimental data.

Despite having different sp^3 fractions, the three quenched networks are still structurally similar. Evidence of this similarity is seen in Fig. 16 which shows the distribution function $G(r)$ for each of the three structures. The three curves are alike in both shape and peak position and represent good fits to the experimental $G(r)$ shown in Fig. 2. Note that the $G(r)$ shown for the instant structure was averaged over a shorter time than the other two structures. Consequently the instant $G(r)$ has more noise and less thermal broadening.

We note that experiment also provides support for our observation that the sp^3 fraction is dependent on the quenching time. It is known that experimentally prepared ta-C is metastable, and hence it is physically reasonable that the structure will change when the formation conditions are varied. Wang and Ho[22] have performed simulations of ta-C using different cooling rates. However, the cooling rates they used correspond to quenching times of 2 and 4 ps, an order of magnitude longer than the cooling times used in this work.

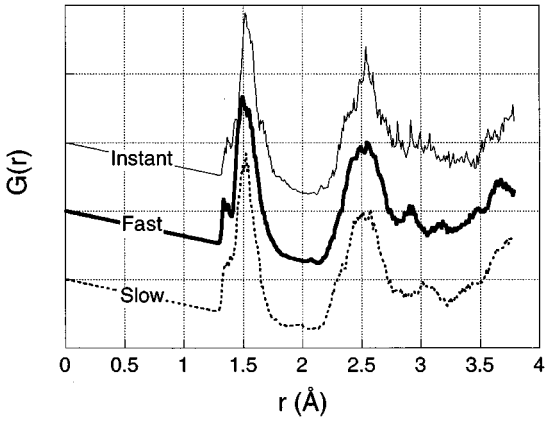

FIG. 16. Distribution function $G(r)$ for the structures generated using the instant, fast, and slow cooling protocols. Note that the $G(r)$ shown for the instant structure represents an average over 0.05 ps, whereas the other two structures are averaged over 0.5 ps. Consequently the instant $G(r)$ has more noise and less thermal broadening.

They found that the sp^3 fraction did not change when the cooling rate was varied, but they did observe a change in the clustering properties of the sp^2-bonded atoms. The absence of a variation in sp^3 fraction in their simulations most likely is a function of the longer cooling times used.

H. Application to theory of film growth

The dependence of the sp^3 fraction on the quenching time has a direct application to theories of how ta-C is formed. It is well known that when ta-C is grown using energetic ion beams, the sp^3 fraction is dependent on the energy of the ions. In particular, the sp^3 fraction is a maximum when the ion energy lies between 40 and 500 eV and slowly decreases as the ion energy is further increased. The most popular explanation for this behavior[17–19] is that at high ion energies the impacting ion damages the growing film which reduces both the film density and the sp^3 fraction. However, while this model is physically plausible, it is based on speculation rather than simulation or experimental evidence.

The results obtained in this simulation are relevant to film growth processes for the following reason. When each energetic ion is deposited, it heats a small surface region in a process known as a thermal spike. This thermal spike, which can be pictured as a high-temperature nonequilibrium liquid, cools by diffusion to the surrounding area. The link between this simulation and experimental film growth processes is that the cooling time of the thermal spike spike increases as the ion energy rises.[51] Thus the use of different quenching rates in this simulation parallels the energy dependence of the cooling rate in the experimental situation.

This connection between simulation and experiment suggests that the experimentally observed decrease in sp^3 fraction can be identified with the downward trend seen in Fig. 14. This link provides an explanation for why the sp^3 fraction decreases when ta-C is prepared experimentally using higher ion energies. It also suggests that the cooling time is an important experimental parameter, particularly in light of the nonequilibrium nature of the thermal spike.

This interpretation is consistent with experiments performed by Cuomo *et al.*,[52] who deposited *ta*-C films onto a variety of substrates having different thermal conductivities. They found that the sp^3 fraction of the films increased with the thermal conductivity of the substrate, demonstrating that the rate of heat removal influences the sp^3 fraction.

No experimental data measuring the spike lifetime is available, but a number of simulations of ion impact have been performed. In particular, a molecular dynamics simulation of carbon film deposition[20] found that for 50 eV ions the cooling time of the thermal spike is of the order of 0.2 ps. In addition, Müller[53] solved the heat diffusion equation using an empirical thermal diffusivity and found that for 150 eV argon ions deposited onto nickel the thermal spike lifetime was approximately 0.2 ps. It is therefore evident that the cooling protocols used in this work represent physically reasonable cooling rates.

IV. CONCLUSION

In conclusion, this *ab initio* study of tetrahedral amorphous carbon presents a number of new results which are in agreement with experiment and provide new insights. In particular, the simulations show that the sp^3 fraction in *ta*-C is dependent on the cooling rate and that the network contains a significant number of three- and four-membered rings which give the network an usual topology.

APPENDIX: SECOND COORDINATION NUMBER CALCULATION

In the literature it is common to find the expression

$$N_2 = N_1(N_1 - 1) \tag{A1}$$

to calculate second coordination numbers N_2 from the first coordination number N_1. This expression is straightforward to derive for any network solid where each atom has a coordination of N_1 and the minimum ring size is 5. A fact not often appreciated, however, is that this relationship is valid only when all atoms have the same bonding environment, that is, when N_1 is an integer. Thus Eq. (6) does not correctly describe materials such as *ta*-C which contain a mixture of threefold and fourfold bonding.

In the case of *ta*-C the correct expression is

$$N_2 = 6(N_1 - 2), \tag{A2}$$

which is derived as follows. Considering the network as containing α sp^2 atoms and $1-\alpha$ sp^3 atoms, the coordination numbers N_1 and N_2 are

$$N_1 = \alpha 3 + (1-\alpha)4 = 4 - \alpha, \tag{A3}$$

$$N_2 = \alpha 6 + (1-\alpha)12 = 12 - 6\alpha, \tag{A4}$$

and by eliminating α we obtain Eq. (7). Note that this calculation assumes the minimum ring size is 5.

The expression defining N_1 requires no explanation but the definition of N_2 in Eq. (9) is more subtle. Every second-neighbor distance can be uniquely identified as being between two atoms which are both nearest neighbors of a third atom. This third atom will be either threefold or fourfold coordinated and from this point of view N_2 is easily calculated as each sp^2 atom will contribute 6 second-neighbor distances while each sp^3 atom results in 12 second-neighbor distances.

[1] D. C. Green, D. R. McKenzie, and P. B. Lukins, in *Properties and Characterisation of Amorphous Carbon Films*, edited by J. J. Pouch and S. A. Alterovitz (Trans Tech, Nedemannsdorf, 1990), Vol. 103.

[2] F. Li and J. Lannin, Phys. Rev. Lett. **65**, 1905 (1990).

[3] G. M. Jenkins and K. Kawamura, *Polymeric Carbons-Carbon Fibre Glass and Char* (Cambridge University Press, Cambridge, England, 1976).

[4] D. R. McKenzie, D. Muller, and B. A. Pailthorpe, Phys. Rev. Lett. **67**, 773 (1991).

[5] P. H. Gaskell, A. Saeed, P. Chieux, and D. R. McKenzie, Phys. Rev. Lett. **67**, 1286 (1991); Philos. Mag. B **66**, 155 (1992).

[6] K. W. R. Gilkes, P. H. Gaskell, and J. Robertson, Phys. Rev. B **51**, 12 303 (1995).

[7] S. D. Berger, D. R. McKenzie, and P. J. Martin, Philos. Mag. Lett. **57**, 6 (1988).

[8] S. R. Elliot, *Physics of Amorphous Materials* (Longman, London, 1984).

[9] N. A. Marks, D. R. McKenzie, B. A. Pailthorpe, M. Bernasconi, and M. Parrinello, Phys. Rev. Lett. **76**, 768 (1996).

[10] R. Car and M. Parrinello, Phys. Rev. Lett. **55**, 2471 (1985).

[11] The calculations have been performed with the code CPMD, version 2.5, written by Jürg Hutter, Max-Planck-Institut für Festkörperforschung, Stuttgart, 1995, with the help of the group for numerical intensive computations of IBM Research Laboratory Zürich and the Abteilung Parrinello of MPI Stuttgart.

[12] D. R. McKenzie, Y. Yin, N. A. Marks, B. A. Pailthorpe, G. A. J. Amaratunga, and V. S. Veerasamy, Diamond Relat. Mater. **3**, 361 (1994).

[13] P. J. Fallon, V. S. Veerasamy, C. A. Davis, J. Robertson, G. A. J. Amaratunga, W. I. Milne, and J. Koskinen, Phys. Rev. B **48**, 4777 (1993).

[14] K. Ogtana, Y. Andoh, and E. Kamijo, Nucl. Instrum. Methods Phys. Res. B **33**, 635 (1988).

[15] F. Rossi, B. Andre, A. Van Veen, P. E. Mijnarends, H. Schut, M. P. Delplancke, W. Gissler, J. Haupt, G. Lucazeua, and L. Abello, J. Appl. Phys. **75**, 3121 (1994).

[16] Y. Lifshitz, S. R. Kasi, and J. W. Rabalais, Mater. Sci. Forum **52& 53**, 237 (1990).

[17] B. A. Pailthorpe, J. Appl. Phys. **70**, 543 (1991).

[18] C. A. Davis, Thin Solid Films **226**, 30 (1993).

[19] J. Robertson, Pure Appl. Chem. **66**, 1789 (1994).

[20] N. A. Marks, D. R. McKenzie, and B. A. Pailthorpe, Phys. Rev. B **53**, 4117 (1996).

[21] J. Tersoff, Phys. Rev. Lett. **61**, 2879 (1988).

[22] C. Z. Wang and K. M. Ho, Phys. Rev. Lett. **71**, 1184 (1993).

[23] T. Frauenheim, P. Blaudeck, U. Stephan, and G. Jungnickel, Phys. Rev. B **48**, 4823 (1993); **50**, 1489 (1994); T. Köler, T.

Frauenheim, and G. Jungnickel, *ibid.* **52**, 11 837 (1995).
[24] D. A. Drabold, P. A. Fedders, and P. Stumm, Phys. Rev. B **49**, 16 415 (1994).
[25] H.-P. Kaukonen and R. M. Nieminen, Phys. Rev. Lett. **68**, 620 (1992).
[26] P. C. Kelires, Phys. Rev. Lett. **73**, 2460 (1994); Phys. Rev. B **47**, 1829 (1993).
[27] O. F. Sankey and D. J. Niklewski, Phys. Rev. B **40**, 3979 (1989).
[28] C. Z. Wang and K. M. Ho, Phys. Rev. Lett. **72**, 2667 (1994).
[29] In Ref. 9 the density was reported as 3 g/cm^3. This value should have read 2.9 g/cm^3, the same as used in this work.
[30] M. M. Golzan, D. R. McKenzie, D. J. Miller, S. J. Collocot, and G. A. J. Amaratunga, Diamond Relat. Mater. **4**, 912 (1995).
[31] J. P. Perdew and A. Zunger, Phys. Rev. B **23**, 1425 (1981).
[32] W. Andreoni, D. Sharf, and P. Giannozzi, Chem. Phys. Lett. **173**, 449 (1990).
[33] S. Nosé, Mol. Phys. **52**, 255 (1984).
[34] H. Bilz and K. Kress, *Phonon Dispersion Relations in Insulators* (Springer, Berlin, 1979), p. 96.
[35] P. E. Blöchl and M. Parrinello, Phys. Rev. B **45**, 9413 (1992).
[36] G. Pastore, E. Smargiassi, and F. Buda, Phys. Rev. A **44**, 6334 (1991).
[37] I. Stich, R. Car, and M. Parrinello, Phys. Rev. B **44**, 11 092 (1991).
[38] D. R. McKenzie, D. Muller, B. Pailthorpe, Z. H. Wang, E. Kravtchinskaia, D. Segal, P. B. Lukins, P. D. Swift, P. J. Martin, G. A. J. Amaratunga, P. H. Gaskell, and A. Saeed, Diamond Relat. Mater. **1**, 51 (1991).
[39] G. Galli, R. Martin, R. Car, and M. Parrinello, Phys. Rev. Lett. **62**, 555 (1989); Phys. Rev. B **42**, 7470 (1990).
[40] S. Iarlori, G. Galli, and O. Martini, Phys. Rev. B **49**, 7060 (1994).
[41] M. Bernasconi, G. L. Chiarotti, P. Focher, S. Scandolo, E. Tosatti, and M. Parrinello, J. Phys. Chem. Solids **56**, 501 (1995); P. Focher, G. L. Chiarotti, M. Bernasconi, E. Tosatti, and M. Parrinello, Europhys. Lett. **36**, 345 (1994).
[42] P. Gomes Dacosta, O. H. Nielsen, and K. Kunc, J. Phys. C **19**, 3161 (1986).
[43] *Introduction to Organic Chemistry*, edited by A. Streitwieser and C. H. Heathcock (Collier Macmillan, London, 1976), p. 608.
[44] D. C. Green, D. R. McKenzie, and P. B. Lukins, Mater. Sci. Forum **52& 53**, 103 (1989).
[45] J. Tauc, in *Amorphous and Liquid Semiconductors*, edited by J. Tauc (Plenum, London, 1974), p. 176.
[46] G. A. N. Connell, in *Amorphous Semiconductors*, edited by M. H. Brodsky (Springer-Verlag, Berlin, 1979), p. 73.
[47] P. D. Swift, Ph.D. thesis, University of Sydney, 1989.
[48] J. Schwan, S. Ulrich, H. Roth, H. Ehrhardt, S. R. P. Silva, J. Robertson, R. Samlenski, and R. Brenn, J. Appl. Phys. **79**, 1416 (1996).
[49] However, sufficient unpaired electrons are present to give *ta*-C a very large spin density compared to other carbon forms.
[50] D. G. McCulloch, E. G. Gerstner, D. R. McKenzie, S. Prawer, and R. Kalish, Phys. Rev. B **52**, 850 (1995).
[51] N. A. Marks, D. R. McKenzie, and B. A. Pailthorpe, J. Phys. Condens. Matter **6**, 7833 (1994).
[52] J. J. Cuomo, J. P. Doyle, J. Bruley, and J. C. Liu, Appl. Phys. Lett. **58**, 466 (1991).
[53] K.-H. Müller, J. Vac. Sci. Technol. A **4**, 184 (1986).